Sensors and Materials, Vol. 35, No. 6 (2023) 1871–1890
MYU Tokyo

S & M 3295

Improvement in Vibration of Hybrid Powertrain with Combined Control Methods

Tian-Syung Lan,[1] Hsiu-Ying Hwang,[2*] Jia-Shiun Chen,[2] and Yingchun Long[1**]

[1]School of Intelligent Engineering, Shaoguan University,
No. 288, Daxue Road, Shaoguan, Guangdong 512005, China
[2]Department of Vehicle Engineering, National Taipei University of Technology,
1, Sec. 3, Zhongxiao E. Rd., Taipei 10608, Taiwan

(Received January 7, 2023; accepted May 15, 2023)

Keywords: two-mode hybrid system, powertrain vibration driving mode, motor feedback control, clutch control

The use of hybrid electric vehicles (HEVs) has become more prevalent than before because of their many merits in terms of energy saving and environmental protection. However, as HEVs use an internal combustion engine (ICE) and electric motors, they also have vibration problems that originate from the inherent ICE structure and/or power transfer shifting between the ICE and the electric motors. To find an appropriate control method for reducing the vibration of HEVs, we simulated vibrations from the power transmission line, elastomers, clutch system, engine damper, half-shaft, tires, damper-bypass clutch, and mode shift clutch of HEVs using the driver, ICE, motor/generator, battery, transmission system, mode shift clutch, damper-bypass clutch, and flexible shaft models. These models were simulated separately with different control methods such as pulse cancellation (PC), mode shift clutch speed control (MCC), damper-bypass clutch engagement control (DBCC), half-shaft oscillation feedback control with proportional integral controller (HOFC-PIC), and the combined control method of PC-DBCC-MCC-HOFC-PIC. MATLAB/Simulink was used for the simulation. Although each method was effective in reducing the vibration of certain parts of an HEV, the combined control method was the most effective in mitigating the vibration. In particular, the combined control method reduced the vibration significantly from the resonance of different parts of the HEV's powertrain, including the flexible shaft, tire, ICE, and mode shift at 5, 11, 16, and 2.5 Hz. The results of this study need to be supplemented with further research but can be used as the basis to set up an effective control strategy for the HEV's powertrain.

1. Introduction

Cars with internal combustion engines (ICEs) have been used for decades. Thus, carbon dioxide (CO_2) contained in the combustion exhaust has been continuously released into the environment and has contributed to global warming considerably. The concentration of greenhouse gases including CO_2 continues to increase in the atmosphere owing to the increasing

*Corresponding author: e-mail: hhwang@mail.ntut.edu.tw
**Corresponding author: e-mail: sgulyc@139.com
https://doi.org/10.18494/SAM4318

ISSN 0914-4935
https://myukk.org/

use of fossil fuels, and global warming has intensified as a result.[1] Energy shortages and increasing environmental awareness have made energy saving and carbon reduction the major issues in the automotive industry, which resulted in the introduction of hybrid vehicles into the market. A hybrid electric vehicle (HEV) has advantages of energy saving and low exhaust gas emission. With its maturing technology, the HEV is considered one of the best solutions to overcome the energy crisis and environmental pollution. HEVs are grouped into three different types depending on their powertrain: series-hybrid system, parallel hybrid system,[2] and series-parallel hybrid system.[3]

The HEV requires diverse driving modes as it uses motors and ICEs at the same time. The difference in torque between an engine and an electric motor results in a deviation between the actual and target output torques during the operation of the HEV. The interruption of power transmission or the fluctuation of the output torque of the HEV causes poor dynamic performance and ride comfort.[4] Ride comfort is important for consumers and manufacturers, and is closely related to noise and vibration while driving a car. Therefore, for the effective operation of the HEV, powertrain control has been studied extensively in recent years. For example, Vu[5] developed a fuzzy control for a series-parallel hybrid powertrain, Yuan *et al.*[6] proposed the energy management of the parallel hybrid powertrain, and Arata *et al.*[7] and Meisel [8] studied the energy management of the series-parallel hybrid powertrain.

Noise and vibration affect the operation and service life of parts of an HEV. Therefore, most of the previous studies discussed noise and vibration from various perspectives. He *et al.*[9] mentioned that the mode shift between ICEs and electric motors reduced both ride comfort and system efficiency. Joseph *et al.*[10] found that low-frequency vibration is the main reason for the reduction in ride comfort. Canova *et al.* proposed the closed-loop control of engine start/stop to reduce the torque fluctuation in engine start-up and idling.[11] The use of a dual-scale command strategy was also suggested for reducing the vibration of the engine and chassis induced when the ICE starts.[12]

The HEV has low-frequency vibration generated mainly by the cylinder movement of the ICE and the inertia of the rotating parts. Thus, when the power of the engine increases suddenly, the vibration intensifies, which leads to an unstable power transmission in the HEV and a decrease in ride comfort. Such vibration can be absorbed partly owing to the vehicle's elasticity and damping. However, this causes power loss and torsional vibration. To reduce the vibration caused by the torque, an elastomer can be added, and the clutch control must be conducted in a sophisticated manner.[13] In shifting operation modes in an HEV, the vibration on the drive shaft can occur owing to an uneven torque distribution in the clutch actuation system. To reduce the vibration, several control methods were proposed using the compensation torque given by the different response times of the electric motor and ICE,[4] and adopting a single planetary gear in which the feedback torque is used to compensate for the vibration.[13] Bypass clutch control was also proposed to reduce the vibration caused by engine start-up.[14]

A smoother and more stable power transmission is necessary to reduce the vibration and improve the efficiency of the powertrain. Therefore, the control logic of the HEV powertrain is required to manage the output torque and reduce the vibration. In the control logic, a feedback command is necessary to offset the vibration along the output axis and control the uneven

torque. In this way, the ride comfort can be improved, and at the same time, the performance of the HEV can be enhanced. Therefore, in this study, we compared different control methods for reducing the vibration and proposed the most appropriate method for HEVs.

2. Materials and Methods

We established a simulation model to test the control methods for a hybrid power transmission system of an HEV. The adopted simulation models included the (1) driver, (2) ICE, (3) motor/generator (MG), (4) battery, (5) transmission system, (6) mode shift clutch, (7) damper-bypass clutch (DBC), and (8) flexible shaft models. The vibration reduction analysis for these models was conducted using MATLAB/Simulink.

2.1 Driver model

To simulate dynamics by different commands during acceleration and deceleration, the driver model was used. In this model, a driving pattern was set up with a target speed considering the resistance in vehicle movement, which was calculated using the preset vehicle speed. The error between the preset and actual speeds of the vehicle was calculated using a proportional integral controller (PIC). The command from the driver when accelerating or decelerating was simulated to monitor the error.

2.2 ICE model

This model was created to simulate the power output from the ICE of the hybrid powertrain. In the HEV, the ICE provides a high torque when the battery capacity is insufficient and more power for the vehicle is required. ICEs provide power in a cycle of intake, compression, explosion, and exhaust. Therefore, a large amount of low-frequency vibration is likely to be generated with a change in pressure in a cylinder. To investigate the vibration of an ICE, the torque provided by gas pressure changes in the cylinder was simulated.[10] The corresponding operation of the single-cylinder mechanism is described in Fig. 1 and Eq. (1).

$$T_E = A_P(P - P_{amb})r\sin\theta_E\left[1 + \frac{r\sin\theta_E}{\sqrt{L^2 - r\sin\theta_E}}\right] \tag{1}$$

Here, T_e, A_P, P, P_{amb}, r, L, and θ_E represent the engine torque of the cylinder (N-m), the piston top area (m^2), the cylinder pressure (psi), the atmospheric pressure (psi), the crankshaft radius (m), the connecting rod length (m), and the crankshaft angle (deg), respectively.

2.3 MG model

According to the required torque and rotation speed, the efficiency of the motor was obtained by using a two-dimensional look-up table and the pre-stored efficiency curve as shown in Fig. 2.

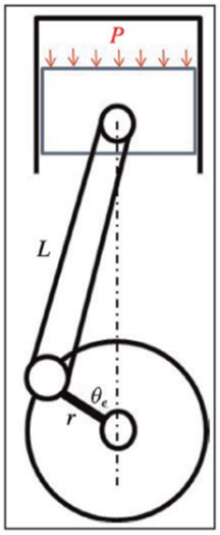

Fig. 1. (Color online) Schematic diagram of operation of single-cylinder mechanism.

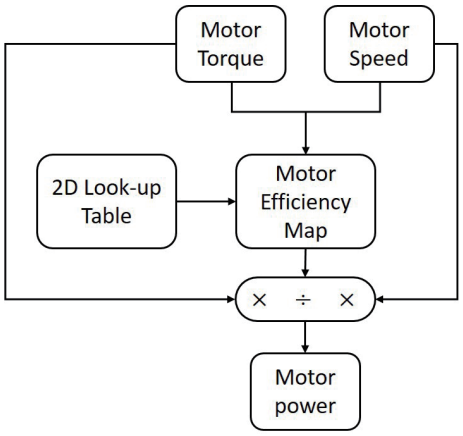

Fig. 2. Diagram of MG model.

2.4 Battery model

The schematic diagrams of the battery circuit and module are shown in Figs. 3 and 4, respectively. The state of charge (SOC) of the battery was calculated on the basis of the number of battery cells connected in series. The battery power was calculated using Eq. (2).

$$P_{batt} = T_{MG1}\omega_{MG1}\eta_{MG1}^{k}\eta_{c1}^{k} + T_{MG2}\omega_{MG2}\eta_{MG2}^{k}\eta_{c2}^{k} \tag{2}$$

Here, P_{batt} is the battery power, η_{c1} and η_{c2} are transformer efficiencies of MG at simulation steps 1 and 2, respectively, k represents the energy flow, and MG represents a motor generator. When the battery is charging, $k = 1$, and otherwise, $k = -1$.

2.5 Transmission system model

We used the two-mode compound power transmission system to construct a transmission system model and present the complete mechanical operation on the basis of mathematical calculations.[15–18] The transmission system had two operation modes changed by speed and acceleration with a combustion engine, two motor generators, two sets of planetary gears, and a battery pack. To accurately calculate the overall torque and rotation speed of each power source, the rotational inertia of each component in the transmission system and the internal force of the gears were considered for understanding the changes in torque and its corresponding angular acceleration.

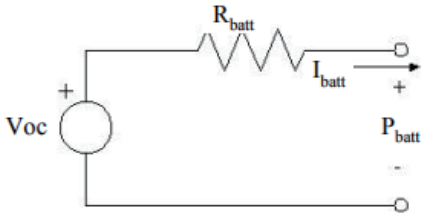

Fig. 3. Schematic diagram of battery circuit.

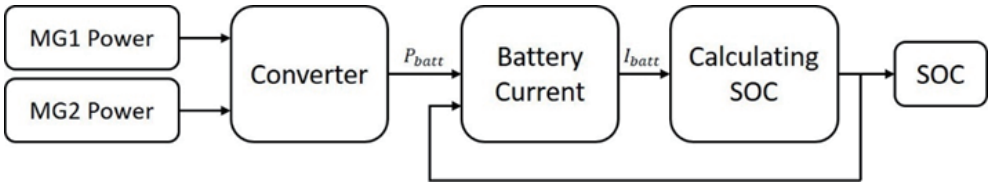

Fig. 4. Schematic diagram of battery module.

2.5.1 Mode 1

Figure 5 shows the transmission system as a free-body diagram. There were three power sources connected to the main planetary gear 2 (P2) through the gears of the compound planetary gear 1 (P1). The power was transmitted to the output shaft to provide power to the whole vehicle. In the figure, RR_1, RS_1, RR_2, and RS_2 are the radii of the ring and sun gears of P1 and P2, respectively. F_1 and F_2 were the internal forces between the planetary pinion, the sun gear, and the ring gear.

2.5.2 Mode 2

Figure 6 shows a free-body diagram of the transmission system in mode 2. In this mode, the clutch (CB12R) was released as the sun gear of P1 and the ring gear of P2 that were connected to each other. Therefore, S1 and R2 run at the same rotation speed.

2.6 Mode shift clutch model

The mode shift clutch model was established to represent the kinetic energy loss caused by the clutch. According to the mode change signal, the clutch engages or disengages while transmitting power. Equation (3) was used to calculate the lost power. The output torque was subtracted from the lost power, and the frictional force loss generated during the release of the clutch was calculated. The schematic diagram of the clutch is shown in Fig. 7.

$$F_{f_k} = \frac{2}{3}\mu_k F_n R \tag{3}$$

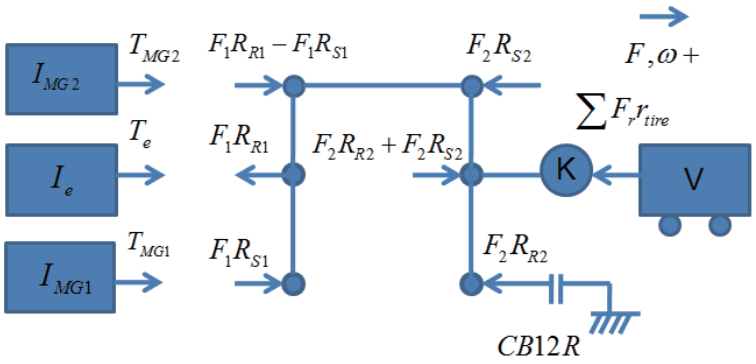

Fig. 5. (Color online) Free-body diagram of transmission system in mode 1.

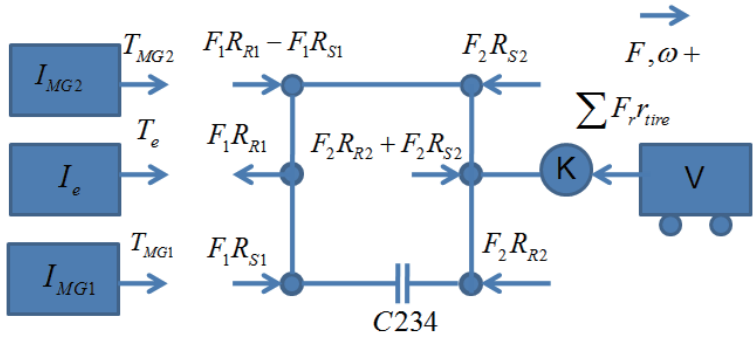

Fig. 6. (Color online) Free-body diagram of transmission system in mode 2.

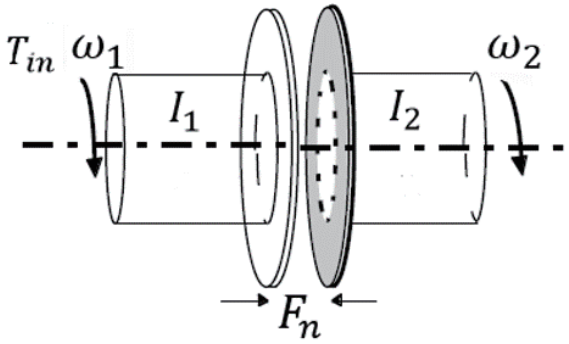

Fig. 7. Schematic diagram of clutch.

Here, F_n, R, F_{f_k}, and μ_k are the normal force of oil pressure, the average surface radius of clutch engagement, the dynamic friction torque, and the dynamic friction coefficient, respectively.

2.7 DBC model

In a conventional powertrain of the ICE, a manual transmission clutch or an automatic transmission torque converter is used between the engine and the gearbox as shown in Fig. 8. In

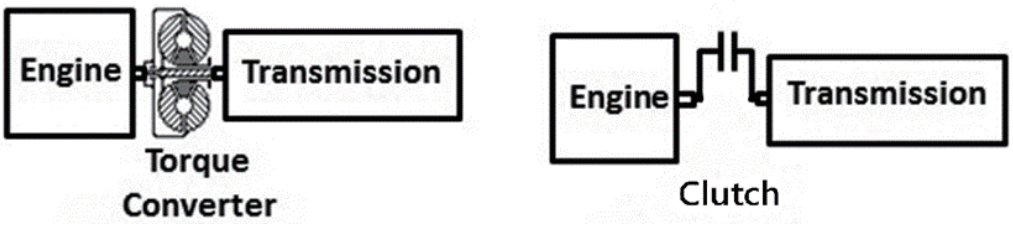

Fig. 8. Schematic diagram of conventional isolation device between engine and gearbox.

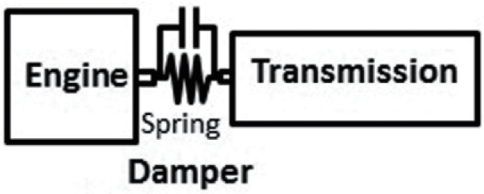

Fig. 9. Schematic diagram of DBC.

the hybrid powertrain, the damper replaces the clutch or torque converters to separate the engine and transmission systems. The damper contained a spring damper and a bypass clutch (Fig. 9). The spring damper acts as a low-pass filter, isolating the high-frequency torque generated by the ICE. However, when an engine starts and stops, the torque fluctuations generated affect the spring damping to oscillate. The DBC, when engaged, bypasses the spring and provides stiffness between the engine and the driveline to reduce damped oscillations generated by the engine during starts and stops. In DBC, the output torque of the engine increases with the normal force generated by the oil pressure of DBC, and the ratio of the distribution output through DBC also increases as shown in Eq. (4).

$$T_{out} = T_{e_{damper}} \left(1 - DBC_{ratio}\right) + T_e \left(DBC_{ratio}\right) - DBC_{friction} \tag{4}$$

Here, T_{out} is the total output torque, $T_{e_{damper}}$ is the output torque via the spring damping of the ICE, T_e is the output torque via oil pressure, DBC_{ratio} is the ratio of the output torque to the total output torque via a DBC and the oil pressure, and $DBC_{friction}$ the frictional force of DBC.

2.8 Flexible shaft model

A flexible shaft model for elastomers such as the axle (half shaft), tires, and ICE damper was established. To show that the elastomer used was subjected to the torsional vibration caused by an external torque, the elastic coefficient and damping were added. The torque exerted on the transmission shaft was calculated using Eqs. (5) and (6) with the transmission system output speed ω_t and the shaft rotation speed ω_{axle}, which were estimated from the vehicle speed.

$$\omega_{gap} = \omega_t - \omega_{axle} \tag{5}$$

$$T_{react} = C_{shaft}\omega_{gap} + K_{shaft}\int_0^t \omega_{gap} dt \tag{6}$$

3. Vibration Control Method

Other than the original control method of the HEV, five control methods were tested and compared in terms of vibration reduction in this study, namely, pulse cancellation (PC), mode shift clutch speed control (MCC), DBC engagement control (DBCC), half-shaft oscillation feedback control with PIC (HOFC-PIC), and the combined control method of PC-DBCC-MCC-HOFC-PIC.

3.1 PC control

In the hybrid powertrain, frequent runs and stops of the ICE occur to increase the vehicle speed. The ICE has an oscillating torque, which may cause vibration and worsen ride comfort. When the HEV is in mode 1 of the transmission system model, the torque is calculated as

$$T_{MG2} = -\frac{R_{R1} - R_{S1}}{R_{R1}} T_E + \left(\frac{R_{S2}}{R_{R2} + R_{S2}}\right) T_{out}, \tag{7}$$

where RR_1, RS_1, RR_2, and RS_2 are the radii of the ring, sun, single planetary, and composite planetary gears, respectively, and T_E, T_{out}, and T_{MG2} are the torque of the engine, the output torque, and the torque of the second MG (MG2).

After that, T_{out} and T_E in Eq. (7) were decomposed into the mean (T'') and oscillation value (ΔT) as shown in Eq. (8).

$$T''_{out} + \Delta T_{out} = -\frac{(R_{R1} - R_{S1})(R_{R2} + R_{S2})}{R_{R1}R_{S2}}\left(T''_E + \Delta T_E\right) + \left(\frac{R_{R2} + R_{S2}}{R_{S2}}\right) T_{MG2} \tag{8}$$

MG2 outputs a torque of the same magnitude in the opposite phase of the first MG (MG1), thereby canceling the oscillation on the driveline.

$$T''_{out} = -\frac{(R_{R1} - R_{S1})(R_{R2} + R_{S2})}{R_{R1}R_{S2}}\left(T''_E + \Delta T_E\right) + \left(\frac{R_{R2} + R_{S2}}{R_{S2}}\right)\left(T_{MG2} + T_{mg2\_f}\right) \tag{9}$$

Here, T_{mg2_f} was the feedback torque given by the control of MG2. T_{mg2_f} and ΔT_E cancel each other in the gear ratio relationship to produce the output torque. Thus, the corresponding torque calculated for the required output is defined as

$$T_{mg2\_f} = -\frac{(R_{R1} - R_{S1})}{R_{R1}} \Delta T_E \tag{10}$$

3.2 MCC

The force generated in the ICE was used as the control variable as the clutch engagement time affected the change in vehicle speed. The clutch engagement time was determined by the speed of the oil pressure increase in the clutch system. After the clutch is fully engaged, the dynamic frictional force is converted to the static frictional force. Therefore, the forces generated by the fully engaged clutch must be considered in the control method. When the static frictional friction is caused by the clutch slip, an incomplete torque output is created to aggravate the vibration of the output shaft. To prevent the clutch slip when it is engaged, the maximum static frictional force must be higher than the generated torque.

3.3 DBCC

DBC generates a signal to engage in power transmission when a start signal from the ICE is received. In this way, the torque is generated when the engine starts, which affects the damping and causes vibration. After the ICE starts and reaches 1600 RPM, DBC outputs the release signal. When the ICE is turned off, DBC receives the engaging signal until the crankshaft of the ICE completely stops rotating and then outputs the DBC release signal. To ensure that DBC does not slip, the frictional force must not be greater than the maximum output of the ICE. Without slipping, no vibration occurs. Since DBC engages in different operational situations, the transmitted torque from the ICE also differs. Therefore, we divided the DBC's engagement into 10 intervals of 10 to 100% of power engagement for the simulation and analysis of vibration. Figures 10 and 11 show the ICE torque diagrams of DBC.

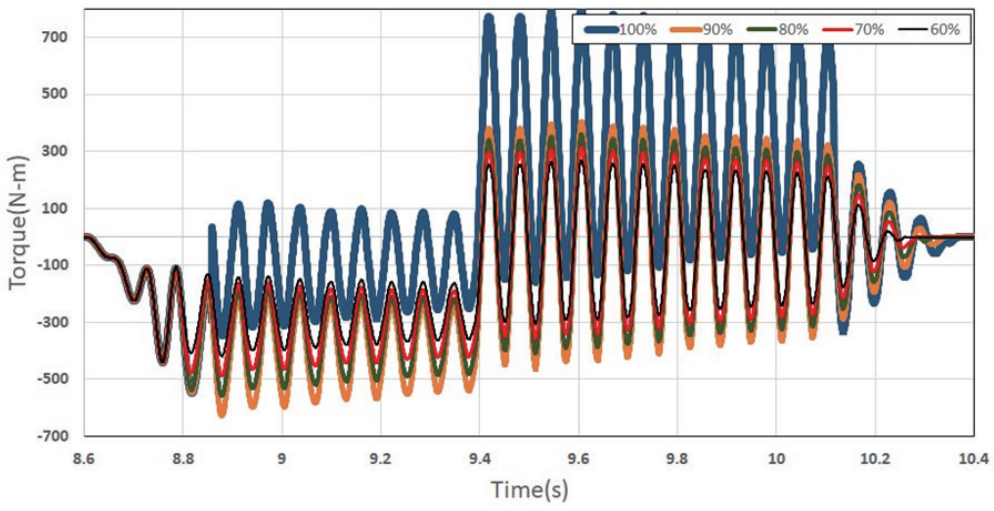

Fig. 10. (Color online) Torque diagram of DBC in 60−100% of power engagement.

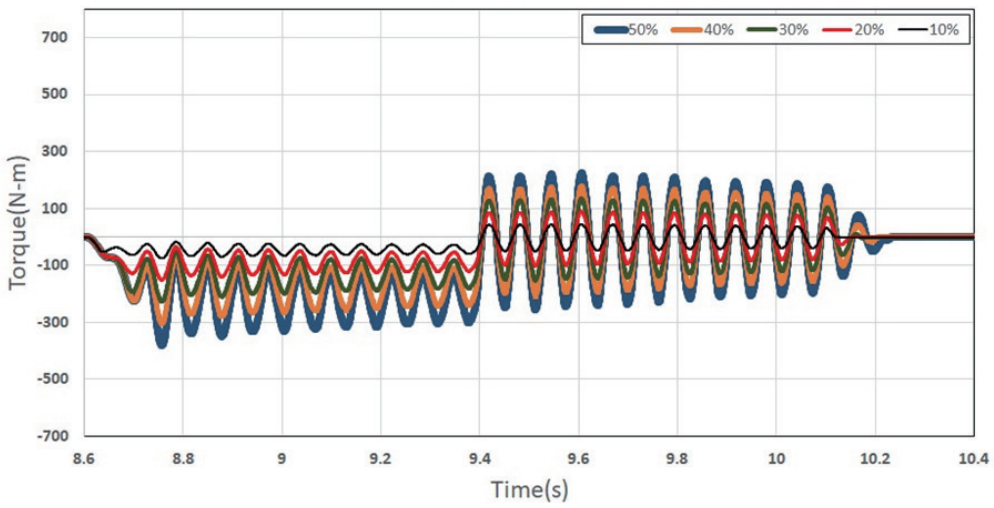

Fig. 11. (Color online) Torque diagram of DBC in 10−50% of power engagement.

3.4 HOFC-PIC

When vibration occurs, the motor provides a corresponding feedback torque to counteract it. At the same time, to meet the power demand, the corresponding rotation speed of the gearbox is calculated on the basis of the current vehicle speed. The calculation is conducted with Eq. (11).

$$N_t = V_{vehicle} / r * (30 / \pi) \tag{11}$$

Here, N_t is the reference rotation speed of the gearbox, $V_{vehicle}$ is the vehicle speed of the previous time step, and r is the effective radius of the tire.

Next, the error value is sent to the PIC to obtain the angular acceleration corresponding to the required vibration-damping torque. The error is calculated with Eqs. (12) and (13). An error value of 0 means that no vibration occurs.

$$\Delta N_t = N_t - N_{t\_exact} \tag{12}$$

$$u = K_p \Delta N_t + K_I \int_0^t \Delta N_t dt \tag{13}$$

Here, N_{t_exact} is the actual rotation speed of the gearbox, ΔN_t is the difference in rotation speed, K_p and K_I are the gain values of PI control, and u is the control effort required for vibration reduction.

4. Results

4.1 Driving cycle

The vibration of the vehicle caused by the driving torque was analyzed in the assumed driving cycle. The driving cycle used in this study was to accelerate from 0 to 72 km/h in the first 15 s and decelerate to 0 km/h after reaching the target speed of 72 km/h (Fig. 12).

4.2 PC

The acceleration curve of the vibration with the original control and PC control is shown in Fig. 13, indicating that the vibration induced when the ICE started and stopped was effectively reduced by PC.

The frequency domain diagram of the vibration with the original control and PC control is shown in Fig. 14. The magnitude of vibration at the damper end of the ICE at 17 Hz significantly decreased by about 20%.

4.3 DBCC

Figure 15 shows the acceleration curve with the original control and DBCC. The engagement of DBCC reduced the vibration by damping when the ICE started and stopped.

The frequency domain diagram (Fig. 16) shows a significant decrease in vibration magnitude at the frequencies of 11 and 16 Hz. The result implies that DBCC was efficient in eliminating the vibration of the ICE.

The simulation results at 10 different levels of DBCC engagement from 10 to 100% show that the optimal level of engagement was 80% to reduce the vibration most effectively with DBCC. The frequency domain diagram shows that the magnitude of vibration was reduced by 10% at the amplitude of 11 Hz, which was the resonance frequency of the tire. Thus, the 80% DBCC engagement was more effective than the 100% DBCC engagement in reducing the vibration (Figs. 17 and 18).

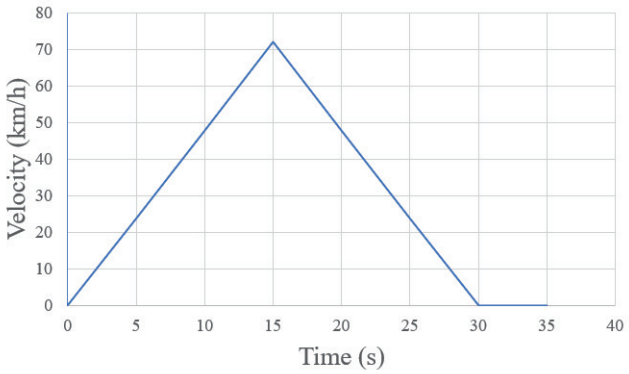

Fig. 12. (Color online) Driving cycle for analysis of vibration.

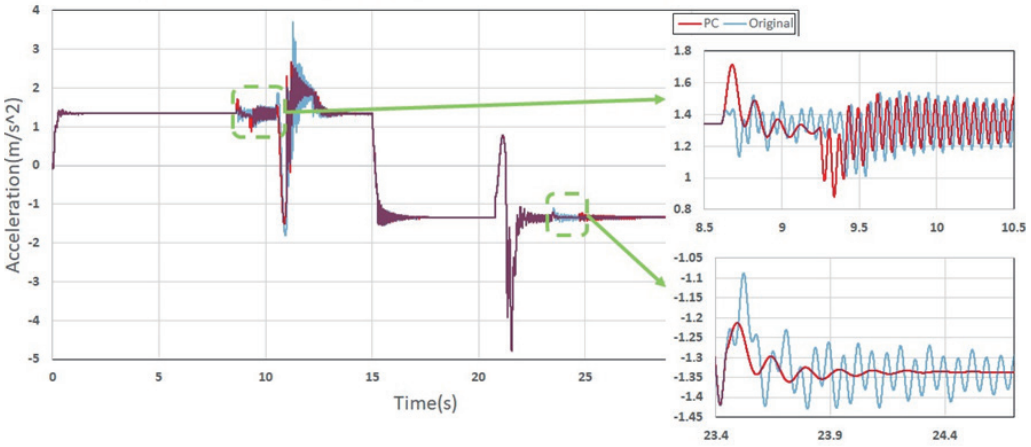

Fig. 13. (Color online) Acceleration curve of original control and PC control.

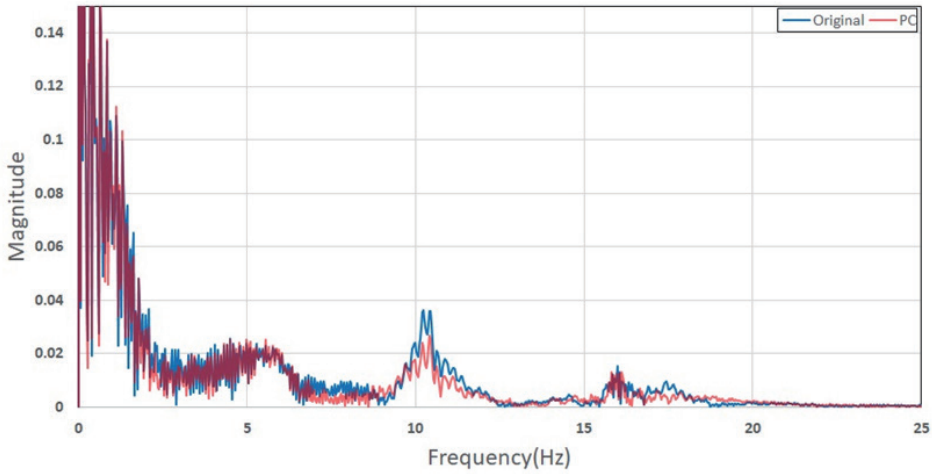

Fig. 14. (Color online) Frequency domain diagram of vibration of original control and PC control (100% engagement).

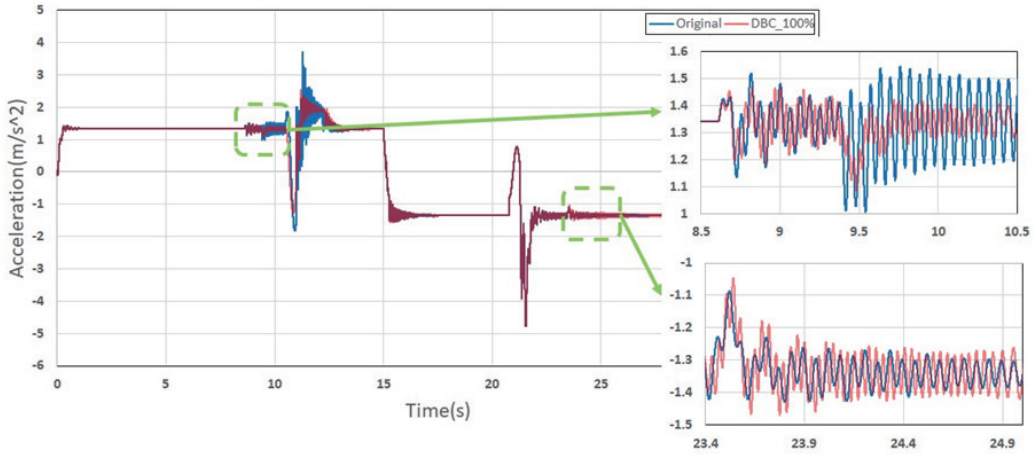

Fig. 15. (Color online) Acceleration curve of original control and DBCC.

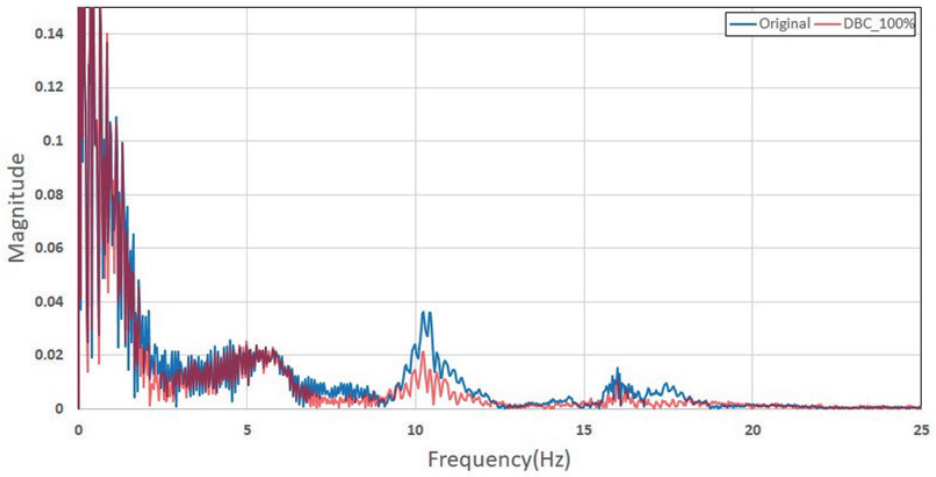

Fig. 16. (Color online) Frequency domain diagram with DBCC (100% engagement).

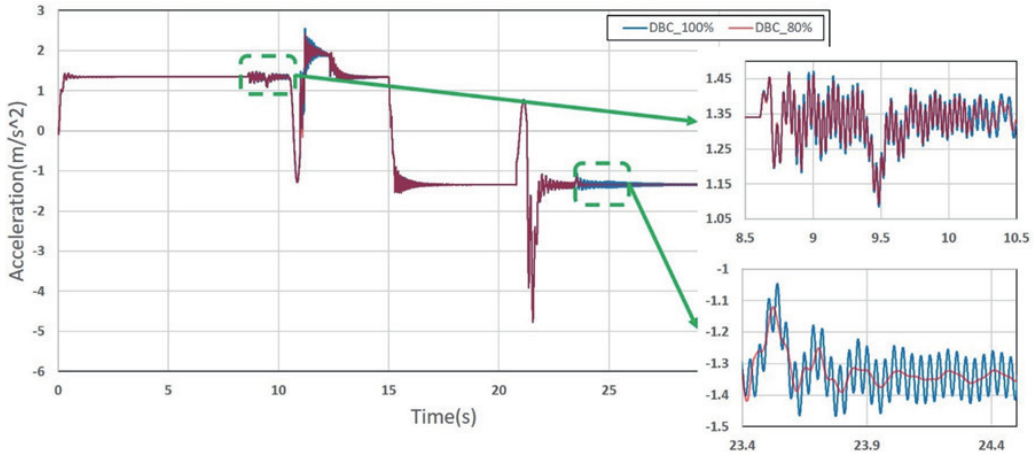

Fig. 17. (Color online) Acceleration curves of 100% and 80% DBCC engagements.

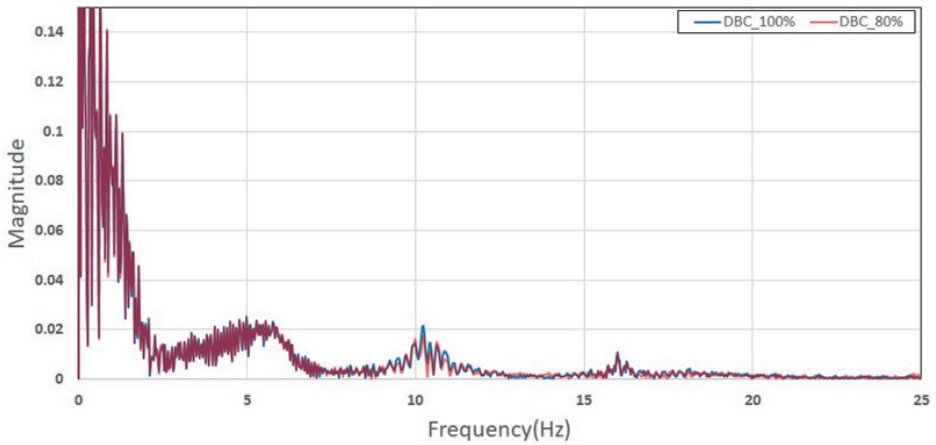

Fig. 18. (Color online) Frequency domain diagram of 100% and 80% DBCC engagements.

4.4 MCC

The mode-switching situation was simulated by controlling the oil pressure of the clutch with MCC. Ten different engagement times from 0.1 to 1 s were used to simulate the effect of vibration reduction. The acceleration curves (Figs. 19 and 20) show that vibration was most effectively reduced at the engagement times of 0.4 and 0.1 s. When the clutch disengaged, the vibration was reduced most effectively at 0.2 and 0.5 s (Figs. 21 and 22).

Figure 23 shows that the resonance of the tire at 11 and 2.5 Hz decreased most significantly. However, the resonance of the ICE damper at 16 Hz did not decrease considerably. As the vibration mainly originated from the ICE, MCC did not decrease the vibration generated by the engine.

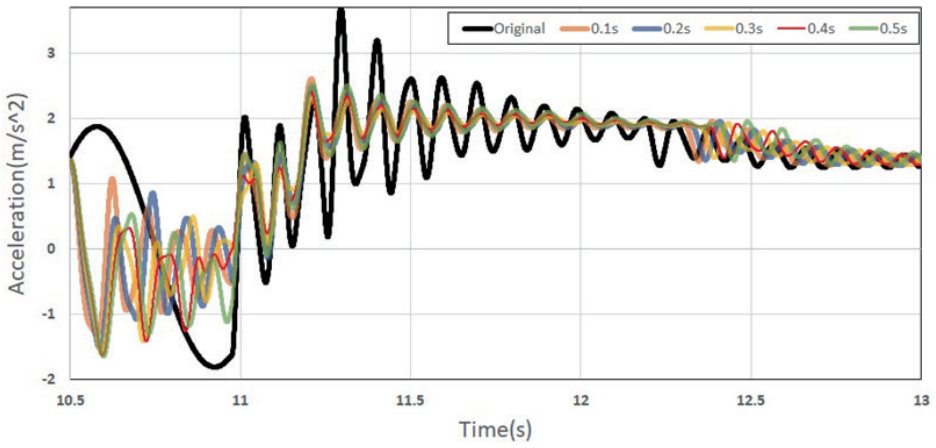

Fig. 19. (Color online) Acceleration curve of MCC with engagement time of 0.1−0.5 s.

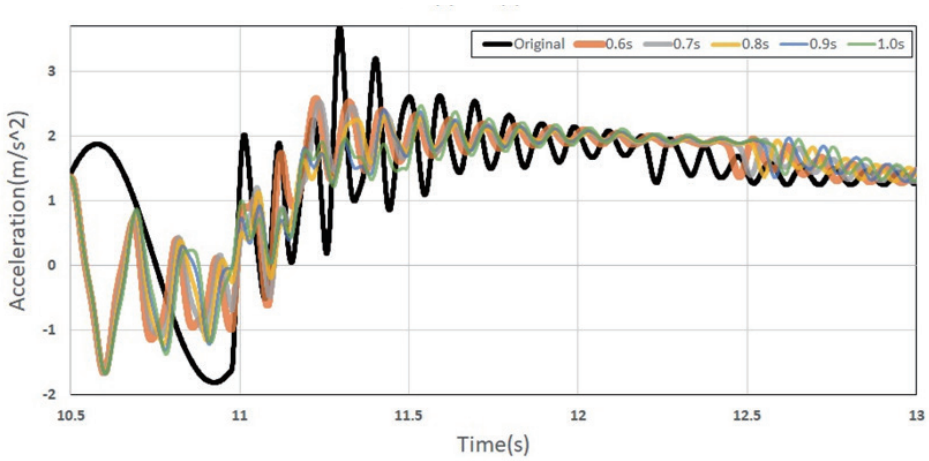

Fig. 20. (Color online) Acceleration curve of MCC with engagement time of 0.6−1 s.

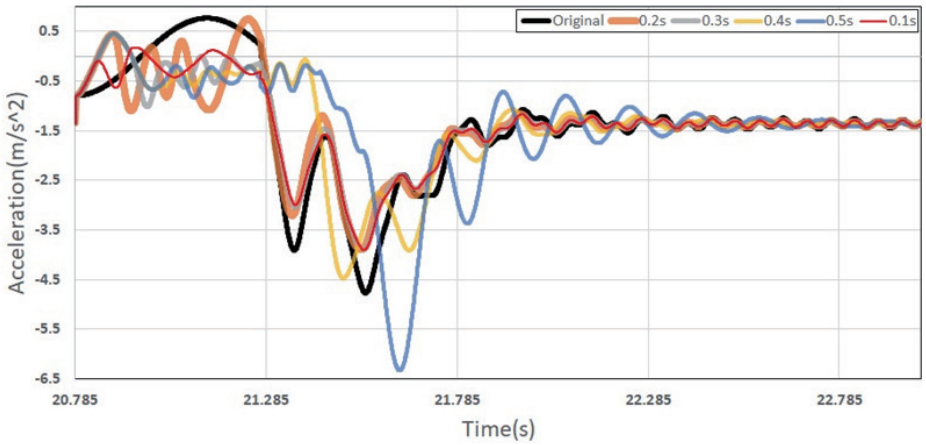

Fig. 21. (Color online) Acceleration curve of MCC with engagement time of 0.1−0.5 s when clutch disengaged.

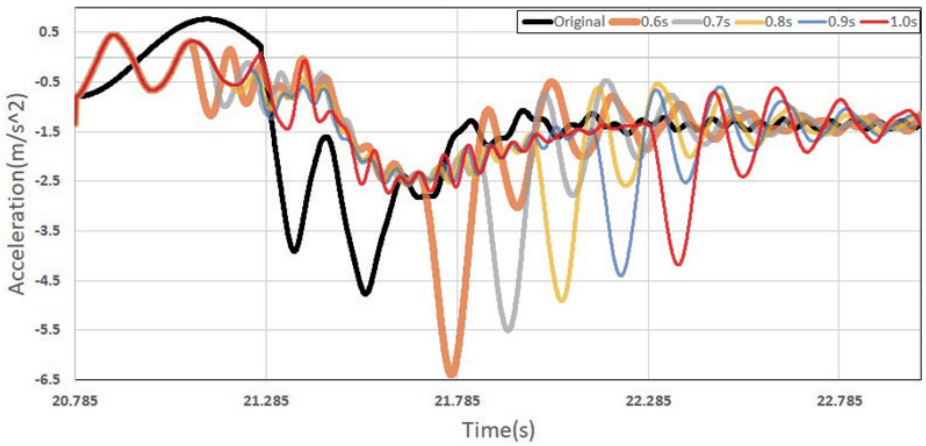

Fig. 22. (Color online) Acceleration curve of MCC with engagement time of 0.6−1 s when clutch disengaged.

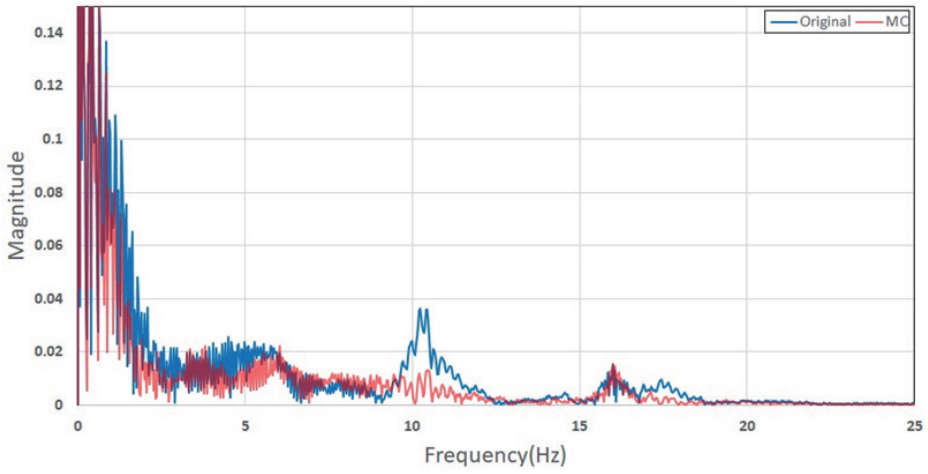

Fig. 23. (Color online) Frequency domain diagram of vibration with original control and MCC.

4.5 HOFC-PIC

When the gearbox causes vibration, the speed of each rotating part needs to be adjusted with the torque of the motor generator for vibration reduction. The difference in vibration acceleration between the original control and HOFC-PIC is shown in Fig. 24. By motor speed adjustment, the vibration acceleration was reduced significantly.

The frequency domain diagram of the vibration with HOFC-PIC shows that the vibration decreased considerably from frequencies of 2 to 12 Hz (Fig. 25).

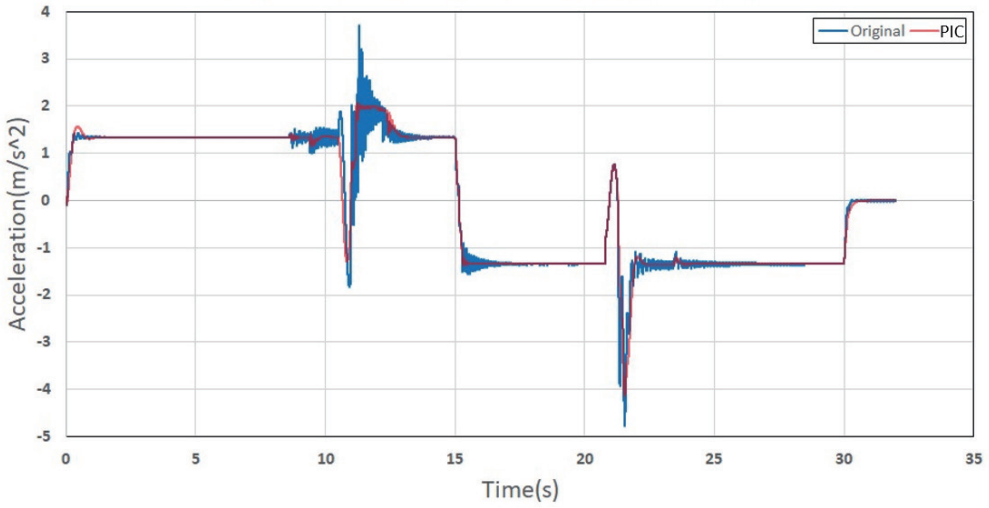

Fig. 24. (Color online) Acceleration curve of HOFC-PIC.

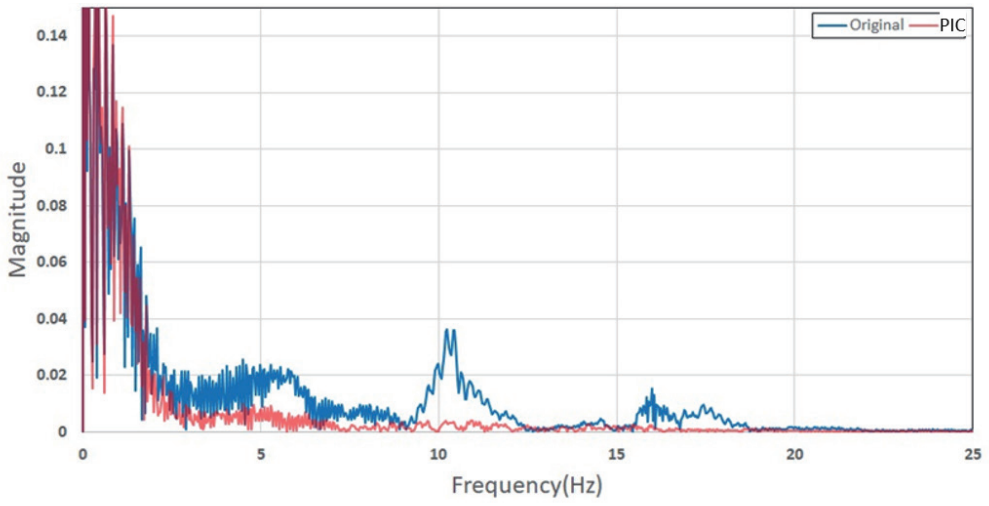

Fig. 25. (Color online) Frequency domain diagram of vibration with HOFC-PIC.

4.6 Combined control method of PC-DBCC-MCC-PIC

PC and DBCC reduced vibrations from the inside of the ICE, which was transmitted along the output axis of the planetary gear. MCC reduced the shock caused by power source switching, whereas PIC reduced the vibration caused by the rotation speed along the output axis in the actual transmission system by controlling motor generators. In addition to controlling the torque of the power source, the half-shaft oscillation also needs to be controlled. Therefore, we combined PC, DBCC, MCC, and HOFC-PIC to determine how much vibration from various parts of the powertrain was reduced. The acceleration curve in Fig. 26 shows significant decreases in vibration with the combined control method compared with the original control.

The vibration reduction was also observed in the frequency domain diagram (Fig. 27). The low-frequency vibration decreased significantly, which proved that the combined control method effectively reduced the vibration of different sources transmitted to the half shaft.

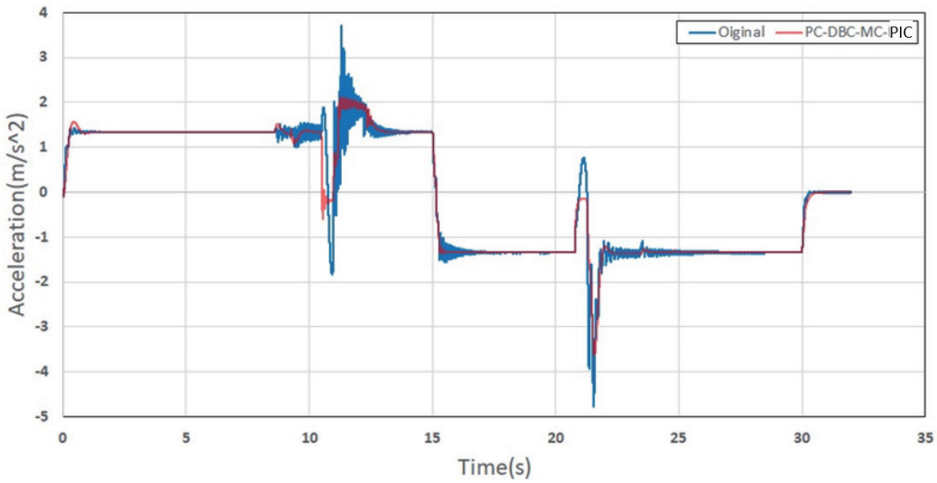

Fig. 26. (Color online) Acceleration curve of vibration with original control and combined control method of PC-DBCC-MCC-PIC.

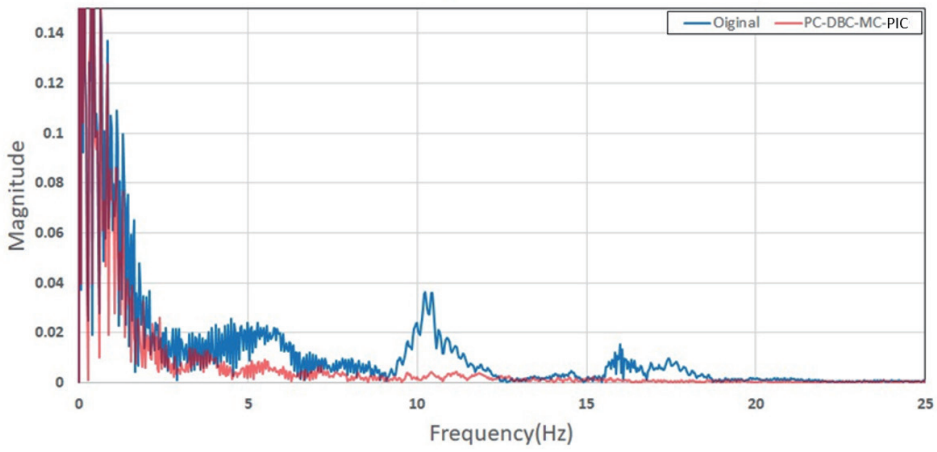

Fig. 27. (Color online) Frequency domain diagram of vibration with original control and combined control method of PC-DBCC-MCC-PIC.

5. Discussion

As shown in Fig. 28, all control methods slowed down the acceleration of the vibration of the ICE. In particular, HOFC-PIC and the combined control method most significantly reduced the acceleration. PC and DBCC with 80% engagement were less effective in reducing the vibration.

The acceleration curve of vibration (Fig. 29) shows that all the simulated controls reduced the vibration. Compared with the original control, the acceleration was markedly reduced by the simulated controls. While PC and DBCC showed a relatively larger acceleration, MCC, HOFC-PIC, and the combined control method reduced the acceleration more effectively in 11 s after shifting the mode of operation. Among them, the combined control method was the most effective in reducing vibration. In shifting modes, only motor generators cause vibration. Therefore, the combined control method is the most effective in reducing the vibration of the engine from the mode shift to the operation of HEVs only by motor generators.

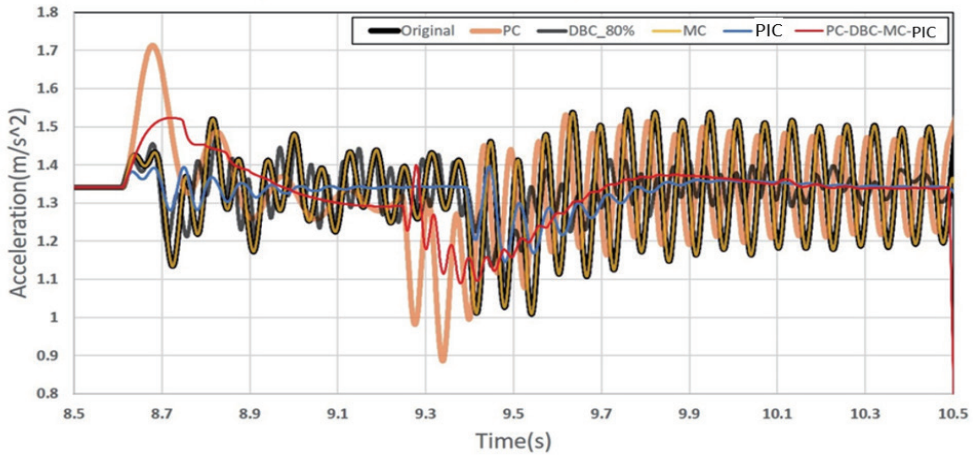

Fig. 28. (Color online) Acceleration curves of vibration of different control methods.

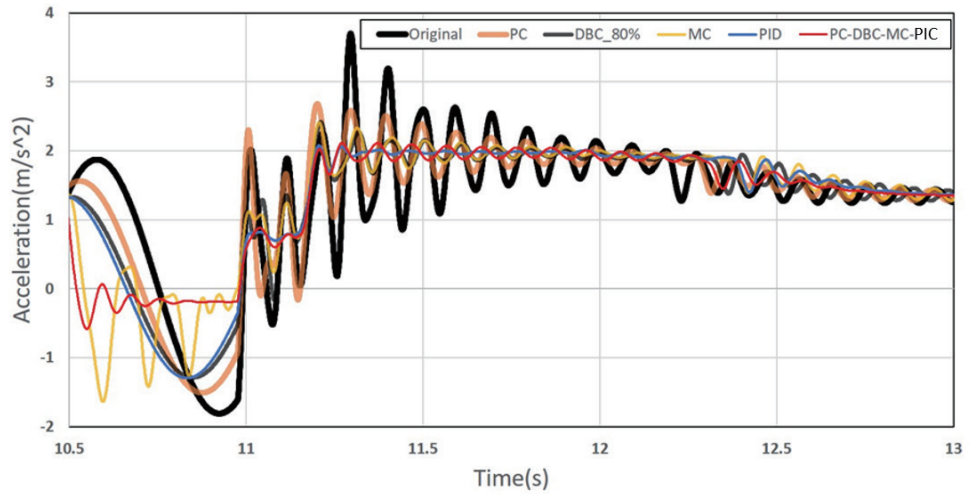

Fig. 29. (Color online) Acceleration curves in shift mode with different control methods.

Table 1
Overall shock absorption and vibration reduction in frequency domain of different control methods.

Control method	PC	DBCC	MCC	HOFC-PIC	Combined control method
Overall vibration reduction	14.2%	34.5%	30%	81.3%	85.5%
Vibration reduction in frequency domain	10% at 11 Hz 5% at 16 Hz	50% at 11 Hz 20% at 16 Hz	30% at 2.5 Hz 65% at 16 Hz	70% at 5 Hz 80% at 11 Hz 80% at 16 Hz	30% at 2.5 Hz 70% at 5 Hz 80% at 11 Hz 80% at 16 Hz

The results show the effects of PC and DBCC in reducing vibration when the ICE starts with combined effects as the two control methods complement each other's deficiencies. When motor generators are used, PC can be used to decrease vibration. While the ICE starts to operate, DBCC can be operated to reduce the vibration generated by the ICE. However, it is impossible to eliminate vibration effectively. Although DBCC does not respond to vibration fast enough, using PC with DBCC showed a higher effect on reducing the vibration generated by the HEV by up to 33%. MCC decelerates the change in rotational inertia during the mode shift. When shifting modes, the vibration caused by the difference in rotation speed decreased by an average of 23%. In the overall vibration reduction, HOFC-PIC showed the highest effect as it controlled the overall power transmission line. In HOFC-PIC, the compensation of the half-shaft rotation speed and power output had the most significant effect on the overall vibration reduction. The combined control method of PC-DBCC-MCC-HOFC-PIC mitigated low-frequency vibration most effectively. In the simulation model, the resonance frequencies of the flexible shaft, tire, ICE, and mode shift were 5, 11, 16, and 2.5 Hz, respectively. The resonance frequencies at 11 and 16 Hz were most effectively suppressed by HOFC-PIC. By integrating the control methods, the vibration from resonance was also significantly reduced even at a frequency of 2.5 Hz.

On the basis of the above results, the vibration reduction effects of each control method were compared (Table 1). The peak-to-peak amplitude was used to calculate the acceleration of the vibration and estimate the overall shock absorption. In the frequency domain, the reductions in the amplitude of each resonance frequency (2.5, 5, 11, and 16 Hz) were compared in the shift mode.

5. Conclusions

The energy crisis and rising awareness of global warming have recently made people more interested in acquiring HEVs than before. For better ride comfort and efficient use of the powertrain, it is necessary to reduce the vibration caused in various parts of the HEV. As the HEV uses an ICE and MGs together, it has the inherent vibration problem of the ICE as well as that caused by shifting power transfer between two different power sources. To find an effective control method to reduce vibration, we simulated vibration with several control methods using different simulation models. The control methods that were simulated and compared included PC, MCC, DBCC, HOFC-PIC, and the combined method of PC-MCC-DBCC-HOFC-PIC. The

simulation models used in this study included the driver, ICE, MG, battery, transmission system, mode shift clutch, DBC, and flexible shaft models. The power transmission line, elastomers, clutch system, engine damper, half-shaft, tires, damper-bypass clutch, and mode shift clutch were considered in the simulation models. For simulation, the MATLAB/Simulink simulation program was used.

The simulation results of the different control methods showed that each method reduced the vibration of the HEV. PC and DBCC effectively reduced the vibration caused by the start of the ICE and the mode shifts between the ICE and MGs. MCC and HOFC-PIC efficiently reduced more than 80% of the vibration caused by rotational inertia during the mode shift in the power transmission of the HEV. The control methods also mitigated the low-frequency vibration caused by resonance at various frequencies. Resonance vibrations occurred at the flexible shaft, tire, ICE, and mode shift at 5, 11, 16, and 2.5 Hz, respectively. The combined control method reduced the resonance vibration most effectively and mitigated low-frequency vibration by up to 80%.

References

1 National Aeronautics and Space Administration: https://data.giss.nasa.gov (accessed March 2023).
2 K. Upendra: https://www.semanticscholar.org/paper/Dual-clutch-transmission-for-plug-in-hybrid-vahicle-Upendra/a103fea2c1d868e27a21f63b4f700ad43d6cca08 (accessed March 2023).
3 K. Bayindir, M. Ali, and A. Teke: Energy Covers. Manag. **52** (2011) 1305. https://doi.org/10.1016/j.enconman.2010.09.028
4 S. Wang, B. Xia, C. He, S. Zhang, and D. Shi: Adv. Mech. Eng. **10** (2018). https://doi.org/10.1177/1687814018775883
5 D. H. Vu: Fuzzy Control Strategy for GM Front Wheel Drive Two-Mode Hybrid Electric Vehicle (National Taipei University of Technology, Taipei, 2013) pp. 20, 28, 31.
6 Z. Yuan, L. Teng, S. Fengchun, and H. Peng: Energies **6** (2013) 4.
7 J. Arata, M. J. Leamy, J. Meisel, K. Cunefare, and D. Taylor: SAE Int. J. Engines **120** (2011) 1286.
8 J. Meisel: SAE Technical Papers, 2009-01-1321, https://www.sae.org/publications/technical-papers/content/2009-01-1321/ (accessed March 2023).
9 R. He, X. Tian, Y. Ni, and Y. Xu: Adv. Mech. Eng. **9** (2017). https://doi.org/10.1177/1687814017715564.
10 F. A. Joseph, J. C. Issac, and T. J. Paulson: Int. J. Sci. Eng. Res. **4** (2013). https://www.ijser.org/researchpaper/Low-Frequency-Vibration-Analysis-on-Passenger-Car-Seats.pdf
11 M. Canova, Y. Guezennec, and S. Yurkovich: J. Dyn. Syst. Meas. Control. **131** (2009) 061005. https://www.semanticscholar.org/paper/On-the-control-of-engine-start-stop-dynamics-in-a-Canova-Guezennec/30b4fafce7611d883a13363c71e1f679961395f3
12 J. J. Wilbanks and M. J. Leamy: J. Dyn. Syst. Meas. Control. **139** (2017). https://doi.org/10.1115/1.4036034
13 Y. Ito, S. Tomura, and S. Sasaki: Proc. 2007. IEEE 33rd Annu. Conf. IEEE Industrial Electronics Society (IEEE, 2007). https://doi.org/10.1109/IECON.2007.4460237
14 J. S. Chen and H. Y. Hwang: Proc. 2013. The Institution of Mechanical Engineers, Part D: Journal of Automobile Engineering (SAGE, 2013) 3. https://doi.org/10.1177/0954407013491184
15 J. Hendrickson, A. Holmes, and D. Freiman: SAE Technical Papers (2009) 0508. https://doi.org/10.4271/2009-01-0508
16 J. Meisel: SAE Technical Papers (2011) 0876. https://doi.org/10.4271/2011-01-0876
17 J. Liu: Modeling, Configuration and Control Optimization of Power-split Hybrid Vehicles (University of Michigan, Ann Arbor, 2007) p. 35.
18 J. Liu and H. Peng: IEEE Trans. Control Syst. Technol. **16** (2008) 3. https://doi.org/10.1109/TCST.2008.919447